JOURNAL OF SPACECRAFT AND ROCKETS
Vol. 41, No. 2, March–April 2004

Development of Advanced Metallic Thermal-Protection-System Prototype Hardware

M. L. Blosser,* R. R. Chen,† I. H. Schmidt,‡ J. T. Dorsey,§ C. C. Poteet,¶ R. K. Bird,** and K. E. Wurster††
NASA Langley Research Center, Hampton, Virginia 23681

A new metallic thermal-protection-system concept has been designed, analyzed, and fabricated. A specific location on a single-stage-to-orbit reusable launch vehicle was selected to develop loads and requirements needed to design prototype panels. The design loads include ascent and entry heating rates, pressures, acoustics, and accelerations. Additional design issues were identified and discussed. An iterative sizing procedure was used to size the thermal protection system panels for thermal and structural loads as part of an integrated wall construction that included the thermal protection system and cryogenic tank structure. The panels were sized to maintain acceptable temperatures on the underlying structure and to operate under the design structural loading. Detailed creep analyses were also performed on critical components of the panels. Four 18-in.-square metallic thermal-protection-system panels were fabricated. A lightweight, thermally compliant support system to connect the thermal protection system to the cryogenic tank structure was designed and fabricated.

Nomenclature

Q	=	activation energy for creep, Btu/(lb mole)
R	=	universal gas constant, 1.986 Btu/(lb mole °R)
T	=	temperature, °R
T_0	=	reference temperature, °R
ΔL	=	expansion of inner titanium thermal-protection-system (TPS) frame, in.
$\Delta L11$	=	axial expansion of tank under single TPS panel, in.
$\Delta L22$	=	circumferential expansion of tank under single TPS panel, in.
ΔP	=	pressure difference, psi
$\dot{\varepsilon}^c$	=	creep rate at temperature T, in./in./s
$\dot{\varepsilon}_0^c$	=	creep rate at reference temperature T_0, in./in./s

Introduction

A PRIMARY goal of NASA is to develop routine, low-cost access to space. Both single-stage-to-orbit and two-stage-to-orbit reusable launch vehicles (RLVs) are being studied as a means of achieving this goal. Many technologies[1] must be developed or enhanced for RLVs to become a viable option for low-cost space access. Unlike the Space Shuttle Orbiter, most orbiters being proposed for fully reusable launch vehicle systems include internal fuel tanks. The integral fuel tanks will result in larger, lower-density vehicles with much larger surface areas than the Space Shuttle Orbiter. This larger surface area must not only be protected from aerodynamic heating, but also can be exposed to damage from low-speed impacts during ground operations, launch and landing, on-orbit hypervelocity impacts from micrometeorites and space debris, and rain erosion from low-altitude portions of ascent and entry flight trajectories. The large surface area combined with requirements to reduce cost, such as reduced maintenance, reduced turnaround time, operation in a wide range of weather conditions, and longer design life, will require significant advances in thermal-protection-system (TPS) development.

Metallic thermal protection systems[2,3] are a key technology that can help achieve the goal of reducing the cost of space access. The inherent ductility and design flexibility of metallic TPS offer the potential for a more robust system with lower maintenance costs than competing systems.

The current paper describes the design, analysis, and fabrication of prototype metallic TPS panels of a new, advanced configuration that functions as part of an integrated TPS/cryogenic tank wall. Design loads and requirements were developed for a specific location on a proposed reusable launch vehicle. An improved metallic TPS design, adaptable robust metallic operable reusable (ARMOR) insulation, was developed based on lessons learned from previous metallic TPS concepts developed during the X-33 program[4] and earlier NASA metallic TPS concepts.[5] The new ARMOR concept has features to eliminate radiation in panel-to-panel gaps, to provide subsurface sealing and attachments, and to decouple deformation and thermal expansion between the inner and outer surfaces. ARMOR TPS panels and associated thermal protection system support (TPSS) were designed to be mounted on an externally stiffened cryogenic tank structure. The insulation in the TPS panels was sized to maintain structural temperatures within acceptable limits. The structural components of the TPS panels were designed and analyzed for acceptable performance under the anticipated aerothermodynamic, acoustic, and inertial loading. Four prototype TPS panels and associated interface hardware were fabricated for future testing.

Loads and Requirements

The objective of the current effort was to design and build realistic prototype metallic TPS panels that would function as part of an integrated cryogenic tank wall system. A specific location on a proposed RLV was chosen as a basis for calculating realistic thermal and mechanical loading histories. TPS design requirements were developed, and loads were calculated for this specific design point.

Reference Vehicle and Structural Component Location

The vehicle and the location on the vehicle selected for design of an integrated TPS/tank component test article were chosen to satisfy specific TPS and tank considerations. A cylindrical cryogenic tank panel was desired to be consistent with previous optimization studies and to be compatible with the Cryogenic Pressure Box Facility, where the integrated component would be tested under combined

Received 13 June 2002; revision received 14 November 2003; accepted for publication 28 November 2003.

*Senior Aerospace Engineer, Metals and Thermal Structures Branch.
†Aeronautical Engineer, Lockheed Martin Space Operations.
‡Aeronautical Engineering Staff, Lockheed Martin Space Operations.
§Senior Aerospace Engineer, Metals and Thermal Structures Branch. Associate Fellow AIAA.
¶Aerospace Engineer, Metals and Thermal Structures Branch.
**Material Research Engineer, Metals and Thermal Structures Branch.
††Senior Research Engineer, Vehicle Analysis Branch. Associate Fellow AIAA.

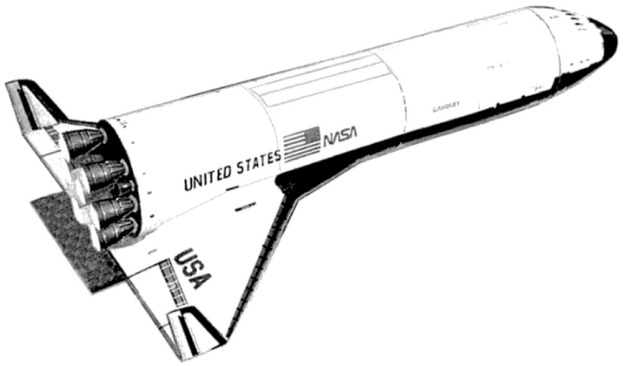

Fig. 1 Wing cylindrical-body reusable launch vehicle configuration.

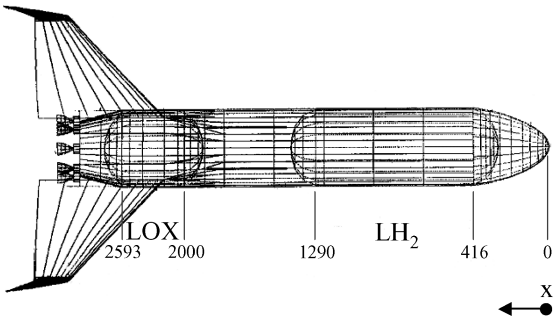

Fig. 2 Wing cylindrical-body vehicle internal packaging and dimensions.

thermal and mechanical loads. It was also desirable to have the test article represent a portion of a cryogenic liquid hydrogen (LH_2) tank to address the integration of TPS and cryogenic tank structure. For the TPS, it was desirable to choose a location as far forward on the vehicle as practical (but behind the carbon-carbon nose cap) where the aerothermal loads (pressures and heating) would be the greatest during entry. Because this is an integrated component, a location was chosen where the TPS was attached to a tank wall. Thus, a location where TPS is attached to the nose fairing or intertank structure would not be acceptable for the current study.

The vehicle chosen as a reference for loads was a wing/cylindrical-body single-stage-to-orbit launch vehicle in the VentureStar™ size and payload class[6] with a gross liftoff weight of 2.9 million lb as shown in Fig. 1. The vehicle configuration has a forward LH_2 tank, a midbody payload bay, and an aft liquid-oxygen (LOX) tank (see Fig. 2). The location on the vehicle for defining the component and corresponding loads is near the LH_2 tank forward-dome/barrel intersection, on the windward side (highest heating) centerline of the cylindrical body, at fuselage station 413 (413 in from nose of vehicle).

TPS Design Requirements

Because the TPS forms the external surface of an RLV, it must be designed for all of the environments experienced by the vehicle.[3] The primary function of the TPS is to protect the vehicle and its contents from aerodynamic heating, and so it must be sized to keep internal temperatures within acceptable limits. In addition, the TPS must maintain its structural integrity so that it provides an acceptable aerodynamic surface during all portions of flight through the atmosphere. The TPS panels must therefore be designed to withstand aerodynamic pressure and drag loads, acoustic and dynamic loading from the engines at launch, dynamic pressures that can cause panel flutter, thermal expansion mismatches between the TPS and underlying structure, and strains induced by primary vehicle loads on the underlying structure. The TPS must also have an acceptable risk of failure after low-speed impacts during launch and hypervelocity impacts from orbital debris in space. Of course, all of these functions must be accomplished while eliminating any unnecessary mass.

In addition to performing all of these thermal and structural functions, the TPS must help reduce overall vehicle costs to enable a viable commercial RLV. Costs can be reduced by lowering initial fabrication and installation costs, reducing required maintenance and repair between flights, reducing turnaround time between flights, and widening the operational envelope of the RLV so that it can spend more time in operation. Therefore, costs can be reduced by developing TPS that requires little inspection, maintenance, and repair between flights and that can enable a vehicle to fly through all but the most severe weather. The specific tradeoff between performance (mass) and cost for TPS must be made for each specific RLV to meet its final set of mission and service objectives. However, a proposed set of general requirements that apply to an external TPS system is described in Ref. 3. The detailed requirements used to size the ARMOR TPS are described in Ref. 7 and summarized here. For the current study, the ARMOR TPS panels were designed for the anticipated thermal and structural loads, but the cost (and implied robustness) requirements were not well defined enough to be used to size the panels.

Flight Envelope and Load Conditions

Applied loads on the vehicle are a direct consequence of the ascent and reentry trajectories flown, the LH_2 and LOX tank internal pressure schedules, vehicle accelerations, vehicle acoustics, etc. A complete flight envelope would be defined by flying ascent/entry trajectories for all expected combinations of vehicle velocity/mass combinations, vehicle missions, and abort scenarios. The full flight envelope would be required for detailed design and optimization of the TPS for the flight vehicle. However, to design the current prototype panels a representative set of load cases were defined from a nominal ascent and entry, as outlined in Ref. 3 and detailed in Ref. 7. The following eight load conditions were used: 1) liftoff (largest acoustic load), 2) ascent with maximum heat flux, 3) ascent with maximum static-pressure differential (largest pressure load on the TPS panel), 4) ascent with maximum temperature gradient, 5) ascent with maximum axial acceleration, 6) entry at the initial occurrence of maximum heating rate (when the TPS panel outer surface generally reaches its highest temperature), 7) entry with maximum static pressure differential (pressure is smaller than during ascent, but panel is warm/hot and properties will be degraded), and 8) entry with maximum temperature gradient. These load conditions were chosen as likely to contain the most severe loading for the metallic TPS panels. However, not all of these load conditions ended up contributing to the sizing of the TPS panels.

Aerothermal Environment and Trajectory

Aerothermal convective heating profiles were developed using the same approach as Ref. 7. Figure 3 shows the ascent and entry surface radiation equilibrium heat-flux history, calculated for a surface emissivity of 0.86, for the chosen location (STA 413) on the wing/cylindrical body RLV. As for most rocket-powered RLV's most of the aerodynamic heating occurs on entry. The entry heating is typical of a trajectory constrained to limit the maximum heating (in this case to avoid overheating the metallic TPS). The maximum radiation equilibrium temperature distribution for entry, calculated

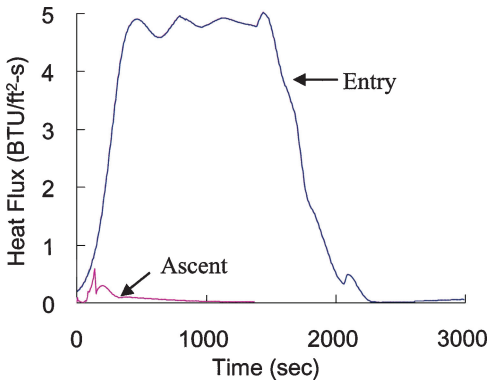

Fig. 3 Surface heat-flux history.

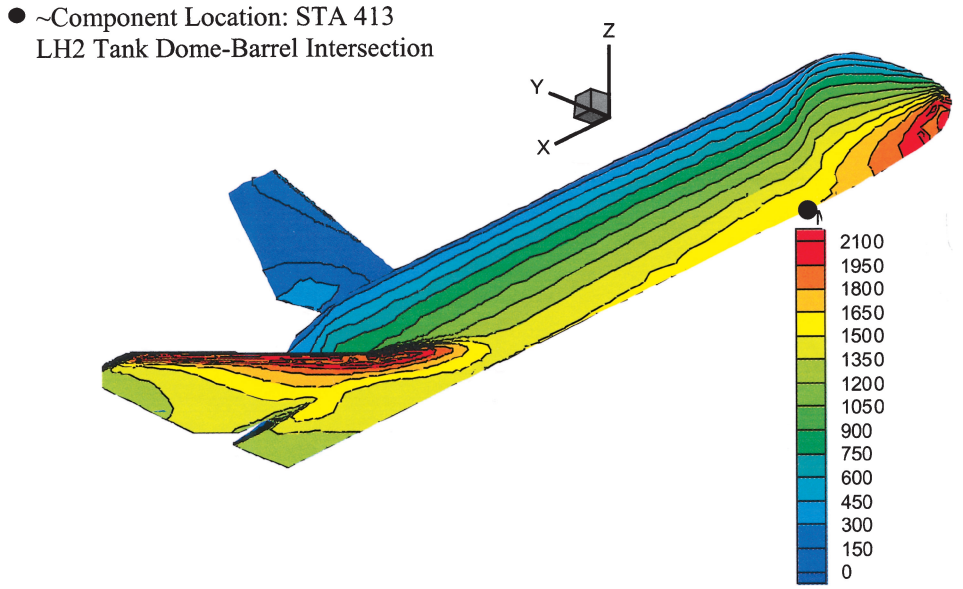

Fig. 4 Maximum radiation equilibrium surface temperatures.

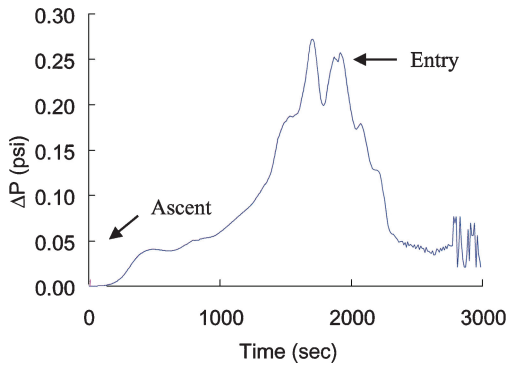

Fig. 5 Pressure loading history.

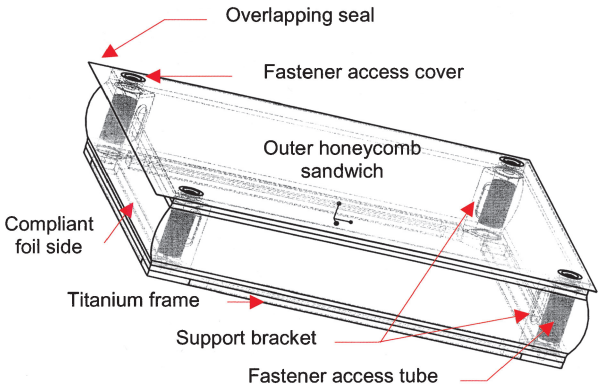

Fig. 6 ARMOR TPS panel.

assuming a surface emissivity of 0.6, is shown in Fig. 4. Although these temperatures are higher than what would be expected for a coated metallic TPS, the figure shows that most of the vehicle surface is well within the maximum temperature range of metallic TPS (approximately 1800–1900°F for Inconel 617).

The predicted static aerodynamic pressure at the vehicle surface is one of the outputs of MINIVER,[8] an engineering code used to estimate the aerothermal environment of entry vehicles. The pressure difference carried by the TPS panel Δp was calculated by subtracting the local ambient atmospheric pressure from the static aerodynamic pressure. (The pressure in the panel interior was assumed to be at the local static pressure.) The resulting Δp for ascent and entry at STA 413 are shown in Fig. 5. MINIVER results are based on compressibility effects in the flow and are not valid at subsonic and transonic flight conditions. Thus, a value of 1.5 was chosen as a cutoff Mach number value, below which MINIVER results were not used. However, the maximum Δp on ascent occurs during subsonic or transonic vehicle speeds (depending on location) where the results in Fig. 5 are not accurate. As a result, the ascent value shown in Fig. 5 was modified using the procedure described in Ref. 3 for the ascent maximum Δp load condition.

Metallic TPS Concept

Metallic TPS offers the potential for many design options. The high-temperature alloys used for TPS are available in a range of different foil thicknesses that can be fabricated and joined into complex structural shapes. Metallic TPS can be integrated with various types of substructure as described in Ref. 3. For a smooth substructure, metallic TPS panels can be directly attached. For externally stiffened structures, a TPSS structure might be required.

TPS Panels

In the current effort, an improved metallic TPS design was developed using lessons learned from previous metallic TPS concepts. Figure 6 shows a sketch of the resulting ARMOR TPS panel. One of the most important components of the ARMOR TPS panel is the outer surface because it forms the outer surface of the vehicle and is directly exposed to the environment. A foil-gauge, Inconel 617 metallic honeycomb sandwich panel was chosen for the outer surface because it can efficiently carry the aerodynamic pressures at elevated temperatures and is resistant to oxidation. Other alloys can offer improved performance but were not available within the schedule and budget of the current effort. The gauges of honeycomb sandwich facesheets can be adjusted to increase the surface robustness at the cost of additional weight.

Another key design issue is sealing between adjacent TPS panels. ARMOR TPS provides three different sealing features:

1) On two edges of the panel, the exterior facesheet of the honeycomb panel extends to overlap the panel-to-panel gap and inhibit ingress of hot gases during reentry.

2) A thin-gauge titanium box beam frame defines the edges of the panel's inner surface. These stiff inner edges can be used to compress a lower-temperature felt seal between the TPS panel and underlying structure.

3) Bulged, compliant sides, made of thin-gauge metal foil, enclose the sides of the TPS panel and block the radiative heat-transfer path

in the panel-to-panel gaps. Radiation in panel-to-panel gaps can degrade significantly the thermal performance of metallic TPS.[9]

The structural connection between the hot outer surface and the cooler inner surface is a classic thermal/structural design challenge. The connection must provide adequate strength and stiffness to transfer the required mechanical loads, yet must not allow too much heat conduction or develop unacceptable thermal stresses from the difference in thermal expansion between the inner and outer portions of the TPS panel. For the ARMOR TPS panel the outer honeycomb sandwich panel is structurally connected to the inner box beam by a thin Inconel 718 metal support bracket at each corner of the panel. The brackets are arranged tangent to a circle about the center of the panel so that they can accommodate the thermal expansion mismatch by flexing, yet resist shear loading. Each bracket is beaded to prevent buckling when loaded in compression. These brackets are the most highly loaded and therefore the most critical components of the ARMOR TPS panel.

Another design issue is the attachment of the TPS to the underlying structure. For the ARMOR TPS panel, cool, subsurface mechanical fasteners were chosen. The mechanical fasteners connect the corners of the inner titanium box beam to the substructure. Compliant, bellows-type tubes provide access from the outer surface to the inner mechanical fasteners. Each fastener access tube is closed off at the outer surface by a snap-in Inconel fastener access cover to provide a smooth outer surface. The interior of the fastener access tube is filled with fibrous Saffil alumina fibrous insulation. One hole in the titanium inner frame through which the fasteners attach to the underlying structure is snug, and the other three holes are slotted to accommodate the thermal expansion mismatch between the inner TPS panel and the underlying structure.

Management of rainwater and moisture is also important for TPS. For the ARMOR TPS, a thin-gauge metal foil closes out the bottom of the TPS panel to make a watertight container for the internal insulation. During both ascent and entry, the static pressure varies between vacuum and 1 atmo. It is important to design the TPS to minimize the difference between the local surface pressure and the internal pressure. A vent, covered by fine mesh, in the metal foil backing allows the TPS internal pressure to be maintained at local atmospheric pressure but prevents liquid water from entering the panel interior. Although water vapor can enter through the single vent, the interior of the panel forms a dead air space with no mass transport mechanism to accumulate condensation beyond the moisture contained in the trapped air.

The primary function of the TPS is to reduce the aerodynamic heating reaching the underlying structure. For ARMOR TPS, the metallic components carry all mechanical loads, so that lightweight, non-load-bearing insulation can be used. The interior of an ARMOR panel is filled with low-density Saffil alumina insulation.

ARMOR TPS Integrated with Tank Structure

In the current study ARMOR TPS was integrated with an externally stiffened composite cryogenic tank structure. A foil-gauge titanium TPSS was developed to connect the ARMOR TPS panels to the cryogenic tank structure.

An ARMOR TPS panel is shown assembled on an externally stiffened cryogenic tank structure in Fig. 7. A TPSS, or interface structure, connects the TPS panel to the caps of the external stiffeners of the tank wall. There are several design considerations for the TPSS: 1) it must be able to transfer mechanical loads from the TPS panel to the tank structure, 2) it must provide a stiff latticework to support a subsurface seal around the perimeter of each TPS panel, 3) it must have provisions to decouple thermal and mechanical strains in the tank structure from those in the TPS panel while not generating additional thermal stresses from its thermal expansion mismatch with either of the other two components, and 4) it must not add too much mass to the system.

The TPSS was made of foil-gauge titanium cold-formed and spot-welded into the shape described subsequently. Each corner was a built-up assembly of titanium sheet with a machined titanium cap to which the TPS panels were mechanically attached. Two arms of the latticework were spot welded to each corner assembly. Two

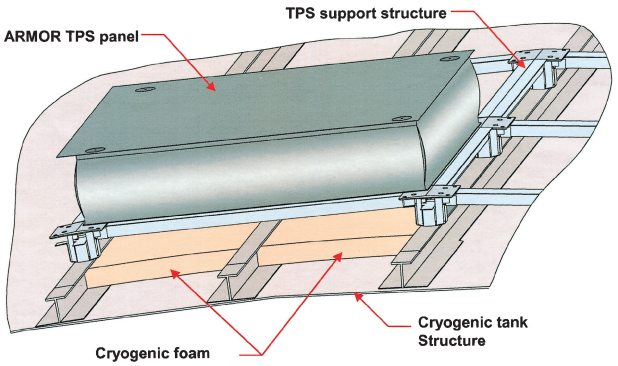

Fig. 7 ARMOR TPS integrated with tank structure.

other receptacles on each corner assembly captured lattice arms from adjacent assemblies while providing a sliding joint to accommodate strain mismatches. Each latticework arm is a titanium sheet box beam spot welded together. The bottom of each corner assembly is mechanically attached to a tank stringer cap.

TEEK[10] cryogenic foam insulation is bonded to the outside of the tank between the stiffeners. When attached to the external stiffeners, the TPS bottom and cryogenic foam surface form a duct that runs along the length of the vehicle. The duct is purged with gaseous nitrogen during vehicle ground-hold to reduce heat flow into the cryogenic fuel tank and to neutralize any potential tank leaks. After reentry and landing an air purge is performed using blowers attached 30 min after vehicle touchdown to cool the blade stiffeners and cryogenic foam insulation surface and to remove heat stored in the TPS panels.

Analysis

Thermal and structural numerical analyses are required to develop the specific loading conditions from the trajectory information, to size the various components of the TPS panels, and to calculate the response of the panels to various thermal and mechanical loads. The generation of specific loading conditions and the thermal and structural sizing of various TPS panel components were performed in an iterative manner to arrive at the final panel dimensions. Detailed structural analyses, including creep and panel flutter,[11] were performed to assess the performance of the resulting TPS panels.

Thermal Finite Element Model

A one-dimensional transient heat-transfer finite element model was created to calculate the temperatures throughout the TPS panel/cryogenic tank assembly and to size TPS Saffil and cryogenic foam insulation layers. Because the TPS panel had not been sized at this point, nominal values were input for the gauges of the various elements of the panel (facesheet thicknesses, core thickness, seal bar dimensions, etc.). Running the model using the heating rates shown in Fig. 3 resulted in sizing of the cryogenic foam thickness on the tank and the fibrous insulation thickness in the TPS panel, as well as calculated temperature histories for all of the TPS panel elements. The temperature Δp and trajectory information were all used to construct the specific applied load cases.

Figure 8 shows a diagram of the finite element model. (Reference 2 demonstrated that one-dimensional models can adequately represent the thermal performance of a metallic TPS panel.) Surfaces are depicted by open circles, and were used to apply boundary conditions and keep track of surface-related quantities, such as coating emittance and surface area. Filled circles represent nodes, and lines represent rod heat-transfer elements. The details of the ARMOR TPS panel, including the honeycomb sandwich on the TPS outer surface, the fibrous insulation, heat shorts from the support brackets, fastener access tubes and compliant sides, and titanium box beam, were modeled using the same approach as Ref. 7.

ARMOR TPS can be mechanically attached to a TPSS that in turn is mechanically attached to the tank external blade stiffeners. TPSS was modeled by increasing thermal capacitance at the node located at the bottom of the TPS. Two elements in parallel, located

Table 1 Vehicle loads at body station 413

Parameter	Load cases							
	Liftoff	Ascent max qdot	Ascent max delta P	Ascent max T1-T2	Ascent max ax	Entry max_qdot	Entry max_delta_P	Entry max_T1-T2
Time, s	6	364	35	105	165	453	1705	2355
Mach	0.05	27.80	0.34	2.30	5.90	26.90	12.20	1.04
Pstatic, psia	1.47E+01	1.69E−05	1.20E+01	9.30E−01	4.90E−02	3.98E−02	2.75E−01	6.00E−01
Patm, psia	1.47E+01	1.69E−05	1.19E+01	8.82E−01	2.77E−02	9.70E−05	3.23E−03	5.50E−01
vehicle_ax, g	0.00E+00	3.00E+00	1.43E+00	1.97E+00	3.00E+00	−1.20E−02	−8.15E−02	−4.10E−02
vehicle_ay, g	0.00E+00	0.00E+00	0.00E+00	0.00E+00	0.00E+00	0.00E+00	0.00E+00	0.00E+00
vehicle_az, g	0.00E+00	7.11E−02	−8.14E−02	8.70E−03	6.49E−02	−1.83E−01	−1.24E+00	−1.06E+00
T1, °F	50	283	48	158	390	1381	1197	103
T2, °F	50	288	50	104	377	1360	1203	156
Tbbeam_top, °F	−85	−63	−85	−86	−81	165	252	287
Tbbeam_bottom, °F	−106	−117	−106	−107	−109	86	171	307
Ttpss_top, °F	−114	−119	−114	−114	−114	76	147	250
T_{tank}, °F	−427	−430	−427	−429	−429	70	86	114
Δp (aero), psia	0.00E+00	0.00E+00	7.00E−02	4.80E−02	2.13E−02	3.97E−02	2.72E−01	5.00E−02
Δp (aero-modified), psia	0.00E+00	0.00E+00	6.09E−01	4.17E−01	1.85E−01	3.97E−02	2.72E−01	5.00E−02
Δp (accoustic), psia	2.77E−01	0.00E+00	2.40E−02	1.00E−02	1.00E−02	0.00E+00	0.00E+00	0.00E+00
Δ Pult, psia	1.16E+00	0.00E+00	9.53E−01	6.26E−01	3.01E−01	5.56E−02	3.80E−01	7.00E−02
Δ Pult-, psia	−1.16E+00	0.00E+00	7.51E−01	5.42E−01	2.17E−01	5.56E−02	3.80E−01	7.00E−02

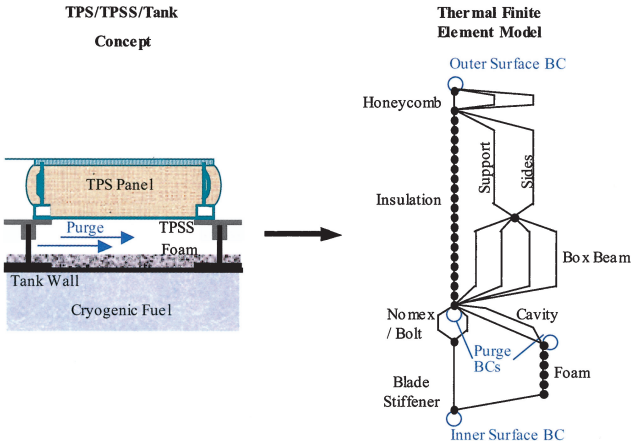

Fig. 8 One-dimensional thermal finite element model of TPS/tank assembly.

between the TPS bottom and the ring frame, were used to model heat transfer through the Nomex felt layer and mechanical fasteners. Heat transfer through the external tank stiffener was modeled with a single element.

A cavity is formed between the back of the TPS panel and the cryogenic foam surface. Heat transfer across the cavity was modeled with two elements in parallel, one modeling gas conduction in an enclosure and the other modeling radiation between infinite parallel plates. Six elements in series were used to model the cryogenic foam insulation layer, and the tank wall was modeled by increasing the thermal capacitance of the innermost node.

Thermal Load Cases

The boundary conditions were varied to represent the thermal conditions expected during the RLV flight cycle. The three transient thermal load cases, ground hold, ascent, and entry, used the same boundary conditions and assumptions listed in Ref. 7. However, the ascent and entry heating histories from Fig. 3 were used in the current analysis.

Insulation Sizing Criteria

Both the Saffil and the cryogenic foam insulation layers were sized using the iterative thermal analysis described in Ref. 7, increasing or decreasing layer thicknesses until an optimum solution was reached. In Ref. 7 a foam-filled honeycomb structure was sized; however, in the current paper an external cryogenic foam (see Fig. 7) was sized with a minimum thickness of 0.25 in. The maximum temperature of the foam was limited to 460°F; however, for the current study this temperature limit did not influence any of the insulation sizing.

Load Table Generation

Critical combinations of thermal and structural loads at several times during ascent and entry were selected as the design loads using an approach similar to Ref. 7. The resulting design loads for windward centerline vehicle station 413 are shown in Table 1. Selected ascent load cases were liftoff, maximum surface heat flux, maximum pressure differential, maximum thermal gradient, and maximum axial acceleration. Entry design load cases were maximum thermal gradient, maximum surface heat flux, and maximum pressure differential. For each load case temperatures, atmospheric pressure, static pressure acting on the TPS surface, and vehicle accelerations were defined. Pressures were calculated using the same approach as Ref. 7.

Thermal-Mechanical Sizing

Sizing of TPS outer sandwich panel layer and insulation layers required iteration between thermal analysis, structural static deflection analysis, and local honeycomb sandwich failure analysis. The process and criteria used are reported in Ref. 7. The liftoff condition, highlighted in Table 1, dictated the structural design of the outer sandwich panel, and was dominated by acoustic pressure during liftoff. Saffil insulation sizing was driven by the reentry heating profile, and cryogenic foam insulation sizing was constrained by the ground hold heat flux into tank criterion.

After the sizing iterations were complete, the following dimensions were obtained. The Saffil insulation thickness was 3.35 in., and the TEEK cryogenic foam insulation thickness was 0.75 in. The outer honeycomb sandwich panel was made of Inconel 617 with facesheet gauge of 4 mils, and honeycomb specification (ribbon gauge × cell size) of 0.002 × 3/16 in. Honeycomb depth was determined to be 0.3 in. Reentry temperature histories for the finalized TPS dimensions are shown in Fig. 9 at three locations inside the TPS/tank system: the TPS surface, TPSS, and tank structure. Dimensions of the prototype hardware, described later, were altered slightly to incorporate available materials and components.

Accommodation of TPS and Tank Expansion

During a flight cycle, TPS and fuel tanks experience extremes in temperatures, from cryogenic temperatures to temperatures in excess of 1400°F. In addition, fuel tank pressures range from 4.0 psig to as much as 35.0 psig. The wide range of temperatures and pressures

Table 2 Calculation of tank and TPS expansions

Load case	Description	T_{TI}, °F	T_{TANK}, °F	Pressure, psi	TPS bolt $\Delta L11$, in.	TPS bolt $\Delta L22$, in.	TPS bottom ΔL, in.	$\Delta L11 - \Delta L$, in.
			Test conditions					
1	Groundhold	70	70	5	0.038	0.005	0.000	0.038
2	Groundhold	−140	−423	5	−0.034	0.019	−0.033	−0.002
3	Groundhold A	−140	−423	14	0.001	0.035	−0.033	0.033
4	Groundhold B	−140	−423	35	0.081	0.072	−0.033	0.114
5	Worst-case heating	250	250	5	0.086	−0.004	0.029	0.057
			Flight conditions					
6	Ascent max fn A	−100	−423	14	0.001	0.035	−0.027	0.027
7	Ascent max fn B	−100	−423	35	0.081	0.072	−0.027	0.108
8	Ascent max T1-T2 A	−100	−423	14	0.001	0.035	−0.027	0.027
9	Ascent max T1-T2 B	−100	−423	35	0.081	0.072	−0.027	0.108
10	Entry max Qdot ($t = 453$ s)	130	70	18.7	0.140	0.019	0.010	0.131
11	Entry max ΔP ($t = 1705$ s)	210	86	18.7	0.143	0.018	0.023	0.121
12	Entry max ΔT ($t = 2355$ s)	300	114	18.2	0.180	0.010	0.038	0.142
13	Thermal soak ($t = 4355$ s)	250	210	4	0.068	−0.003	0.029	0.039
			On orbit					
14	A	−250	−250	18.7	0.037	0.039	−0.048	0.086
15	B	250	250	18.7	0.214	0.005	0.029	0.185

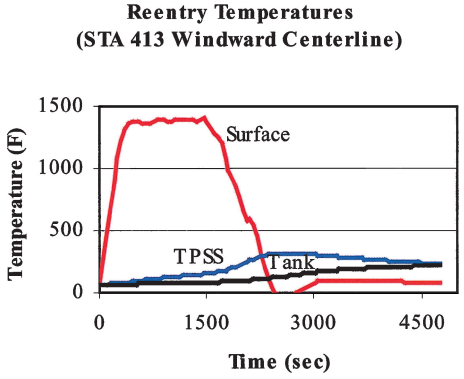

Fig. 9 Entry temperature histories.

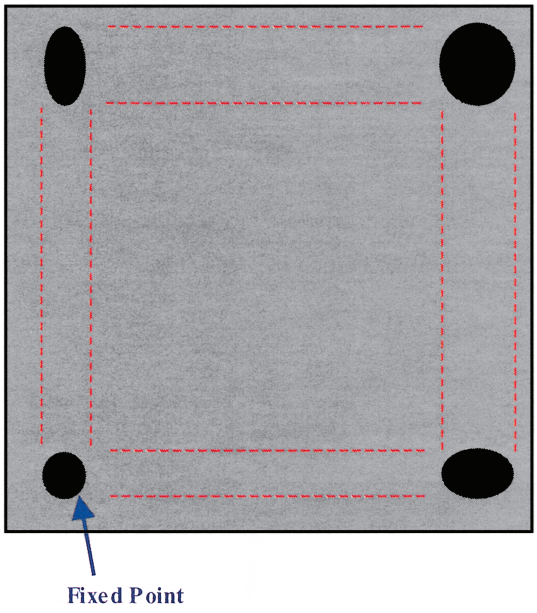

Fig. 10 Expansion slot pattern on bottom of titanium TPS frame.

results in differences in expansion and contraction of the TPS and tank that must be accommodated to avoid damage to the TPS.

To determine the expansions expected in the system, a table of load cases (Table 2) was created recording the temperatures and pressures at various times during the vehicle flight cycle. For each load case the temperature of the tank and the titanium inner surface of the TPS and the tank pressure are listed. The displacements of the tank under a single TPS panel in the axial and hoop directions, the displacement of the inner TPS surface, and the difference between the tank and TPS displacements are also listed in Table 2.

The 15 load cases are grouped into three categories. The category labeled "Test conditions" represents conditions expected during testing of the integrated test article, which combines the ARMOR TPS, TPSS, and a representative tank structure. The category labeled "Flight conditions" represents conditions expected for the wing/cylindrical body RLV during ascent and entry. Finally, the category labeled "On orbit" represents estimated bounds (A and B) of on-orbit temperature and tank pressures.

Tank expansions were calculated assuming a 14-ply IM7/977-2 composite tank using ±65-deg ply orientation. It was further assumed that the axial external blade stiffener height was 3 in. Tank expansion in the 1 and 2 direction (axial and hoop) are reported in the columns labeled "TPS Bolt $\Delta L11$" and "TPS Bolt $\Delta L22$," which represents the tank growth over an 18-in. span, the size of a single TPS panel. The term "TPS Bolt" signifies the TPS attachment bolts that mechanically attach the TPS at the four bottom corners to the external stiffeners.

The motion of the TPS bolts is directly coupled to the motion of the tank. The bolt at one corner of the TPS frame is fixed, as shown in Fig. 10, but the bolts in the other corners are allowed to move as a result of expansion slots in the TPS bottom frame. The expansion slots are designed to constrain the translational and rotational degrees of freedom of the TPS panel while allowing free expansion relative to the tank. The required dimensions of the expansion slots were determined by plotting the quantities $\Delta L11$-ΔL and $\Delta L22$-ΔL, as shown in Fig. 11.

Support Bracket Design

As already discussed, the corner support brackets are the most highly loaded and critical structural components of the ARMOR TPS panel. Each bracket has the conflicting requirements to 1) provide an adequate structural connection between the outer honeycomb sandwich and the inner titanium frame, 2) limit the heat conduction between the hot outer surface and the cooler interior, and 3) accommodate the thermal expansion mismatch between the outer Inconel surface and the inner titanium frame. The basic design approach was to use a thin metal strip that could bend easily in one direction but not in other directions. The metal strips were located in the corners of the panel and arranged to be tangent to a circle about the center of the panel. In this way the outer honeycomb and

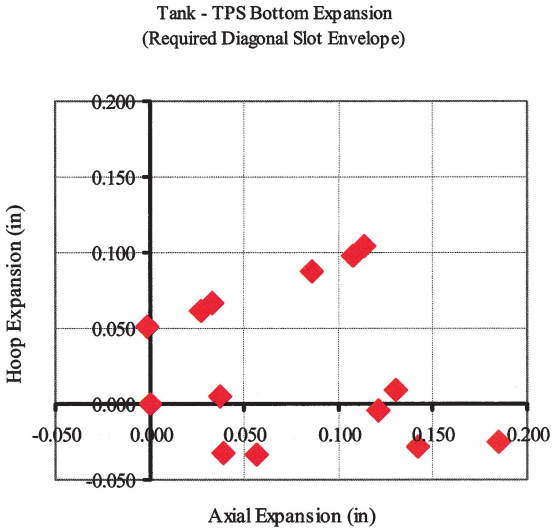

Fig. 11 Plot of tank expansion relative to TPS expansion.

the inner frame were free to expand thermally about the center of the panel with little resistance from the brackets connecting them. However, the brackets also had to resist compressive aerodynamic loading, and so a stiffening bead was placed in the middle of the bracket, away from the ends, to prevent buckling. The ends of the bracket remained flexible enough to accommodate the thermal expansion mismatch. The bracket was made thin to reduce the amount of heat conducted from the outer surface to the interior and to keep the bending stiffness and stresses low.

Selecting the width, thickness and bead geometry for the brackets was not straightforward. A number of candidate geometries were chosen and analyzed with detailed finite element models to find one that was an acceptable compromise between the conflicting requirements.

The finite element analysis was completed using MSC/PATRAN[12] and MSC/NASTRAN.[13] Two critical load cases, using preliminary loads higher than those in Table 1, were analyzed for each bracket configuration: a hot load case and a cool load case. The hot case simulates a condition during reentry with the maximum surface temperature and negligible aerodynamic pressure. The peak temperature at the hot end of the bracket used for this analysis was 1533°F. For the 18-in.-square TPS panels, the thermal expansion mismatch between the outer surface at the maximum temperature and the inner titanium frame results in a displacement of 0.2 in. at the hot end of the bracket. For the cool load case the bracket must carry a compressive load resulting from a 2 psi pressure load on the outer surface.

One of the configurations analyzed was found to have acceptable stress levels with the least cross-sectional area. The resulting dimensions of the bracket were 1 in. wide, 3 in. long, and 0.025 in. thick. The material selected for the bracket was Inconel 718 because it has high yield stress and good creep resistance at elevated temperatures.

Typical results of the finite element analysis of the selected bracket geometry are shown in Figs. 12 and 13 for the two load cases. Displacements and stress distributions are shown for both load cases.

Typical results for the cool load case are shown in Fig. 12. The deformed shape indicates bracket bending under the applied compressive load. The maximum stress is 76 ksi, well below the 140-ksi yield stress of Inconel 718 at room temperature. The critical buckling load was calculated to be 2.1 times the load, so the bracket is safe from buckling under the 2 psi pressure loading.

Typical results for the hot load case are shown in Fig. 13. The deformations show the transverse displacement at the hot end of the bracket, which accommodates the expansion of the outer hot Inconel honeycomb sandwich. The maximum stress is 40 ksi, which is below the 50-ksi yield stress for Inconel 718 at 1600°F.

The bracket configuration was later modified to eliminate the bent ends. The straight ends are brazed into machined fittings, which

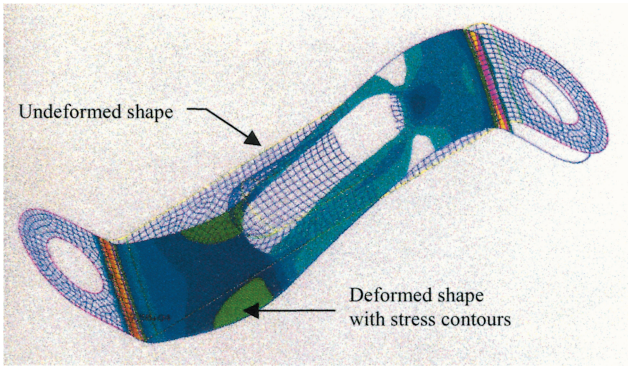

Fig. 12 Typical bracket deformations and stresses for cool load case.

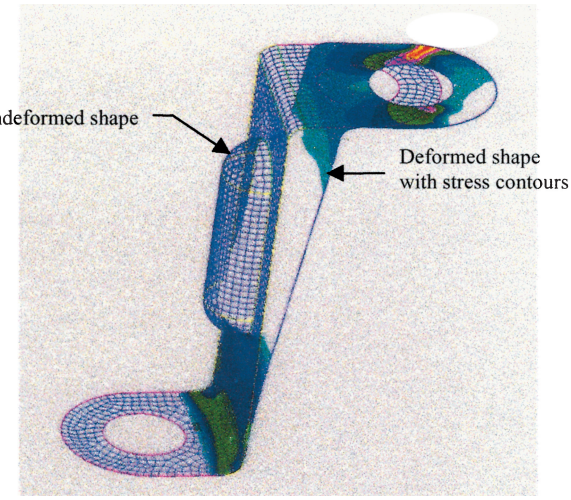

Fig. 13 Typical bracket deformations and stresses for hot load case.

eliminates some of the bending in the bracket and simplifies its shape. The modified support bracket shape was analyzed in subsequent creep analyses.

Creep Analysis

Creep deformation is a concern because the outer Inconel honeycomb sandwich and the four corner brackets react aerodynamic pressures while at elevated temperature. A NASTRAN finite element analysis was performed to investigate the occurrence of permanent deformations caused by creep, creep rupture, and creep buckling.

The phenomenon of creep occurs when the strain in a material continues to increase under constant load. There are generally three different stages of creep. Primary creep is transient creep during which the creep rate decreases over time. As the material deforms, the material strengthens via strain hardening, thus increasing the creep resistance and causing the decreasing creep rate observed. Primary creep gradually transitions into the second stage, referred to as steady-state creep in which the creep strain rate is a constant. The third stage is called tertiary creep and is characterized by an increasing creep rate.

The creep rate is dependent on the stress, temperature, and time. The creep strength refers to the maximum employable stress level for the material at a prescribed temperature. This value of stress corresponds to a given level of creep (for example, 1% creep strain in 10,000 h).

At the macroscopic level, the creep phenomenon is best observed in the uniaxial test under constant load and the relaxation test under constant strain at constant temperature. A specimen subjected to a constant uniaxial tension at an elevated temperature exhibits three distinct phases in a time frame: primary creep, secondary creep, and the tertiary creep to rupture. If the specimen is unloaded after

some creep deformation, the elastic strain is immediately recovered, and a portion of the creep strain is gradually recovered. For metals, recoverable creep strain is generally negligible.

NASTRAN utilizes a creep analysis capability using a generalized viscoelastic model. The formulation is based on the step-by-step time integration of the Kelvin–Maxwell rheological model with nonconstant parameters. If the plastic deformation is coupled with creep, the algorithm will seek a solution in two distinct steps. A number of empirical creep laws, recommended by the Oak Ridge National Laboratory, are provided along with options for general tabular input of the rheological model parameters as functions of effective stress. When the creep characteristics are specified in terms of empirical creep laws, the program converts the empirical formula to the corresponding rheological model.

The NASTRAN creep analysis required either a creep law, such as an empirical exponential law, or tabular data and the calculated stresses. From the temperatures and the maximum stresses calculated in the finite element analysis, the rupture life can be estimated from creep properties for the materials used. If this rupture life is greater than the operation time (including a safety factor), the structure will be considered safe for creep. Alternatively, the time to reach 1% creep strain can be determined, to see whether it is greater than the operation time. If so, the structure will also be considered as safe for creep.

The components of the ARMOR TPS panel modeled for creep analysis consist of Inconel 617 honeycomb sandwich and Inconel 718 brackets. The 18-in.-square honeycomb sandwich panel (with 0.004 in.-thick facesheets and 0.3 in.-thick core) is modeled as a three-layer laminate. The bracket dimensions are 3 in. long by 1 in. wide by 0.02 in. thick with a bead. By taking advantage of two planes of symmetry in the ARMOR TPS panel, only $\frac{1}{4}$ of the honeycomb panel and a single bracket are represented in the finite element model. The TPS panel is assumed to carry 0.52-psi inward acting pressure load at 1750°F for 0.36 h each mission. This loading is more severe than the station 413 loads of the current study, but was considered representative of loads for metallic TPS used nearer to its upper temperature limit.

Creep properties for Inconel 617 and 718 were obtained from Ref. 14. For Inconel 718 creep properties were not available over the entire temperature range of interest. The following temperature effect correction equations[15] were used to extrapolate the creep rates over the desired temperature range:

$$\dot{\varepsilon}^c \Big/ \dot{\varepsilon}_0^c = X^{(T_0/T-1)}$$

where

$$X = e^{(-Q/RT)}$$

The energy of activation for creep can be determined graphically by plotting the natural logarithm of the minimum creep rate on the ordinate against the inverse of the absolute temperature on the abscissa. The slope of the isostress lines is equal to $-Q/R$.

Results of the NASTRAN creep analysis of the ARMOR TPS panel with Inconel 617 brackets are shown in Figs. 14–17. Results are shown for static temperature and load, residual stresses and deformations after a single mission, and stresses and deformations during and after 7 h of loading at elevated temperature (approximately 20 missions). In all of the plots, the deformations are greatly exaggerated for display.

Figure 14 shows the stress contours superimposed on the deformed shape resulting from the applied temperature and pressure loading with no creep. As expected, the center of the panel (the corner opposite the bracket in this quarter symmetry model) deflects inward under the applied pressure loading. The hot end of the bracket is deflected radially outward from the panel center by the thermal expansion of the outer Inconel honeycomb sandwich. The peak stress of 52 ksi results from bending of the bracket near the hot end.

Figure 15 shows the residual stress distribution superimposed on the deformed shape of the panel after one mission. There is some inward residual deflection of the center of the panel. The bracket is

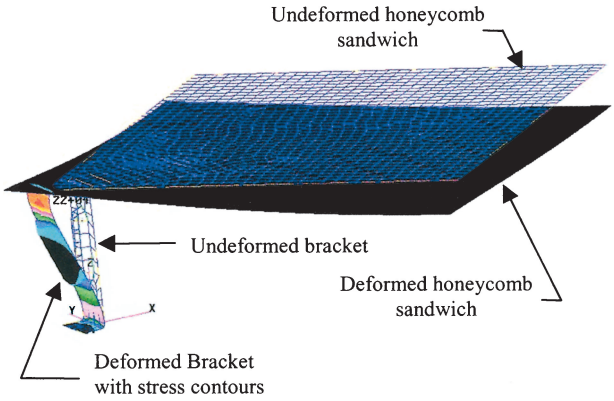

Fig. 14 Stress distribution for static load and temperature.

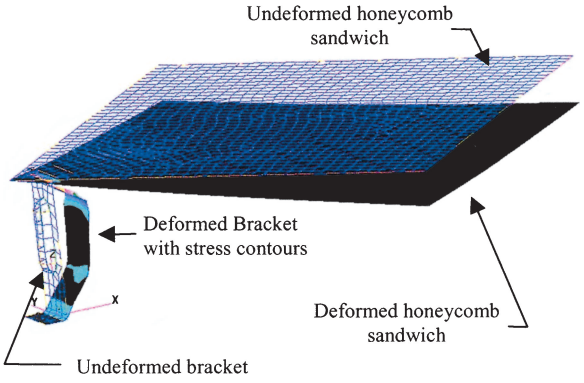

Fig. 15 Stress after first mission.

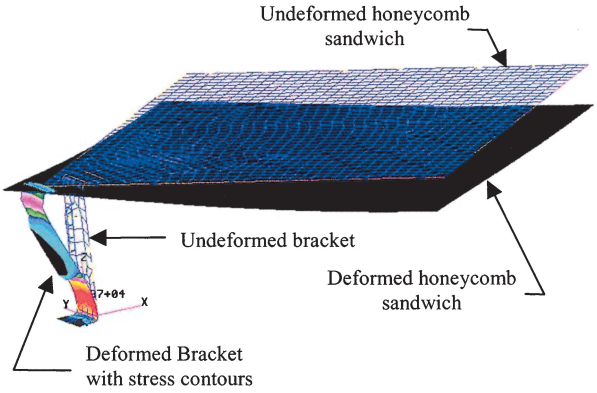

Fig. 16 Stress distribution after 7 h of loading.

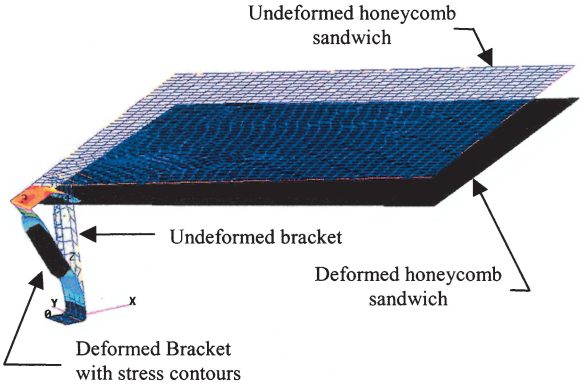

Fig. 17 Residual stresses after 7 h of loading.

bent at both ends so that it bows inward. The highest stresses (up to 35 ksi) are localized near the hot end of the bracket.

Figure 16 shows the stress distribution superimposed on the deformed shape of the panel after 7 h of load at elevated temperature (approximately 20 missions). This stress distribution is shown while the panel is still at elevated temperature and under pressure loading. The deformation pattern and stress distributions are similar to those in Fig. 14; however, the distribution in the bracket is different. The peak stress is reduced to 35 ksi and is located near the cool end of the bracket. The peak stress near the hot end of the bracket is reduced to about 22 ksi.

Figure 17 shows the residual stresses superimposed on the deformed shape of the panel at room temperature under no load after 7 h of exposure to elevated temperature loading. The center of the panel is displaced inward approximately 0.02 in. The flat portion of the hot bracket has developed a slight outward kink with a displacement of less than 0.03 in. The peak residual stress of 32 ksi is located near the hot end of the bracket.

The MARC program[16] was also used to investigate the behavior of an ARMOR TPS panel with Inconel 718 brackets. MARC offered the capability of user-written subroutines to readily incorporate the creep property extrapolations required for Inconel 718. This finite element model was used to define a temperature/pressure boundary, below which the current design has acceptable creep behavior. An example of one of the analyses used to develop the boundary is shown in Fig. 18. The figure shows the deformation of the panel at the onset of creep buckling of the bracket after 17.6 h (approximately 49 missions) at 1700°F and 0.65 psi. The location of the creep buckling is at the same location as the kink observed in Fig. 17.

The predicted boundary of acceptable creep behavior for a current design of an ARMOR TPS panel with Inconel 718 brackets is shown in Fig. 19. The area under the curve labeled "Acceptable" indicates that the panel was able to withstand the combination of temperature and pressure without violating any of the following conditions for the 100 mission life of the vehicle: 1) no creep buckling of the bracket and 2) permanent deflections less than 1% of the diagonal span of the panel to maintain a smooth aerodynamic surface. The load conditions defined in Table 1 are well within the acceptable range.

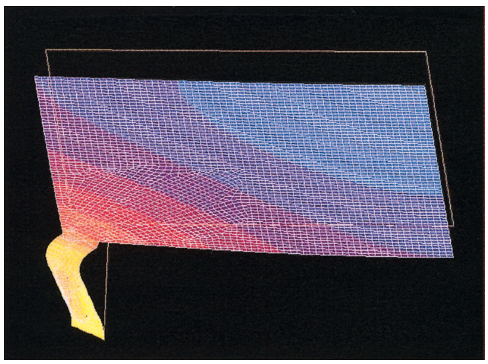

Fig. 18 Deformation at the onset of creep buckling.

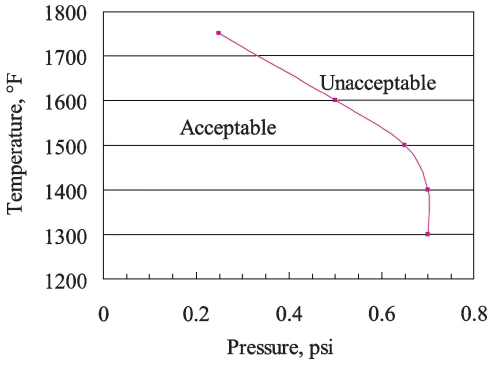

Fig. 19 Creep boundary for current ARMOR TPS panel design.

There is very little creep in the honeycomb sandwich, and almost all of the creep limitations are occurring in the bracket. Therefore, it might be possible to expand the temperature/pressure envelope by further refinement of the bracket design.

Fabrication and Testing

TPS Panels

Four TPS panels with nominal dimensions of 18 × 18 × 3.5 in. were fabricated by BF Goodrich (BFG) Aerospace, Aerostructures Group, using the design already discussed. However, because of cost and scheduling constraints some material and foil gauge substitutions were made. A picture of one of the TPS panels is shown in Fig. 20. Each TPS panel consisted of an Inconel 617 honeycomb core sandwich panel on the top side (hot side), titanium alloy base (cool side), Inconel 625 standoffs and bolt access tubes, Saffil insulation, and a hybrid of Inconel 600, and commercially pure titanium (CP Ti) foil edge closeouts. Details of the brazing and superplastic forming processes used for panel fabrication are proprietary to BFG and are not reported in this paper. The weights for the as-fabricated panels are listed in Table 3.

Figures 21 and 22 show different views of the honeycomb core sandwich panel with corner inserts, standoff brackets, and bellows tubes installed. The honeycomb core sandwich panel for the hot surface was fabricated by brazing 0.006-in.-thick Inconel 617 foil face skins to an 18 × 18-in. Inconel 617 section of honeycomb core. The honeycomb core blanket was 0.25 in. tall and had 3/16-in. corrugated square cells with 0.0015-in.-thick cell walls. The face skins on the external surface had a 1-in. overhang along two edges of the honeycomb core to allow for overlapping seals with adjacent TPS

Table 3 As-fabricated ARMOR TPS panel weights

Panel number	Weight, lb	Area weight, lb/ft^2
1	5.17	2.30
2	5.63	2.50
3	5.44	2.42
4	5.41	2.41
Average	5.41	2.41

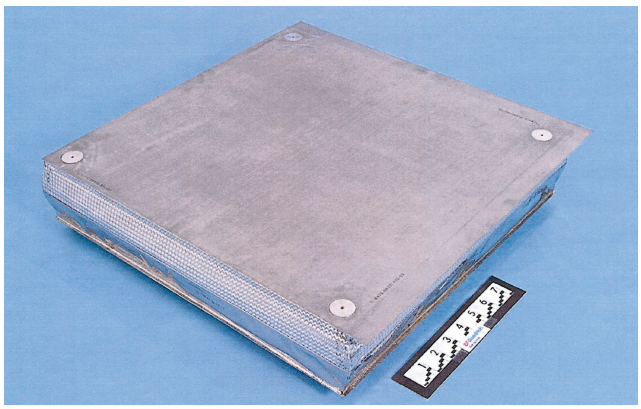

Fig. 20 As-fabricated ARMOR TPS panel.

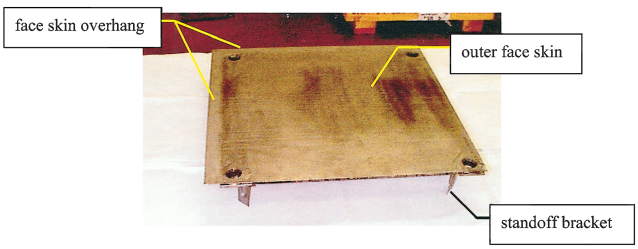

Fig. 21 Inconel 617 honeycomb core sandwich panel with standoff brackets attached (top view).

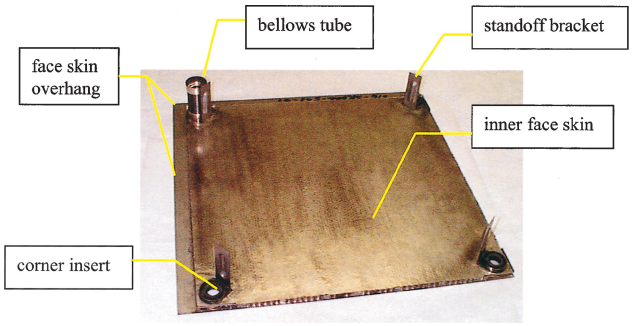

Fig. 22 Inconel 617 honeycomb core sandwich panel with standoff brackets and one bellows tube attached (bottom view).

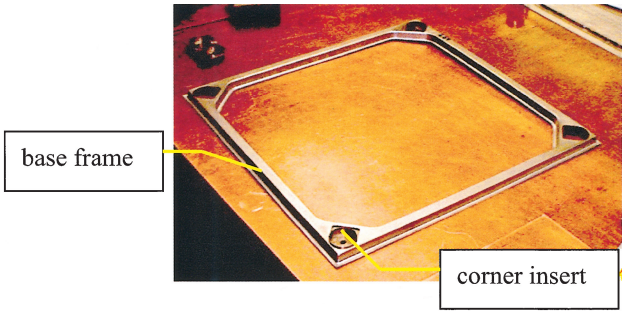

Fig. 23 Ti-6Al-4V base frame cut from superplastically formed pan, with corner inserts installed (top view).

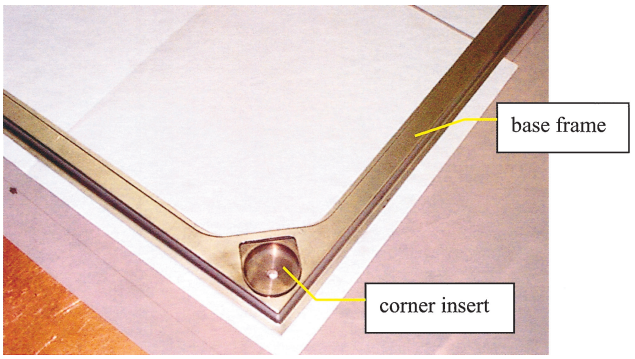

Fig. 24 Enlarged view of corner insert installed in Ti-6Al-4V base frame.

panels when installed on the vehicle. Access holes were cut into the four corners of the sandwich panel, and Inconel 625 inserts were installed into the holes. Three-in.-long Inconel 625 standoff brackets and bellows tubes were brazed to the corner inserts in the honeycomb core sandwich panel. The standoff brackets set the internal dimension of the panel to allow 3.25 in. of insulation to be installed. The bellows tubes serve as seals for the bolt access holes through which the base of the panel will be bolted to the TPSS or vehicle structure.

Figure 23 shows the base frame of the panel that was fabricated using superplastic forming of 0.010-in.-thick Ti-6Al-4V sheet to form a pan. The frame was cut out of the pan. Holes were cut into the four corners of the frame, and Ti-6Al-4V inserts were installed (see Fig. 24). These corner inserts in the base frame were brazed to the free ends of the bellows tubes and standoff brackets to form the skeleton of the TPS panel, as shown in Fig. 25.

Once the TPS panel skeleton was assembled and brazed together, Saffil fibrous insulation with density of 3 lb/ft^3 was installed into the panel's 3.25-in. cavity. A 0.002-in.-thick sheet of CP Ti foil was brazed to the frame to close out the bottom of the base. A 1-in.-diam hole with fine-mesh screen was incorporated into the center of the base closeout foil to allow venting of the TPS panel during service in

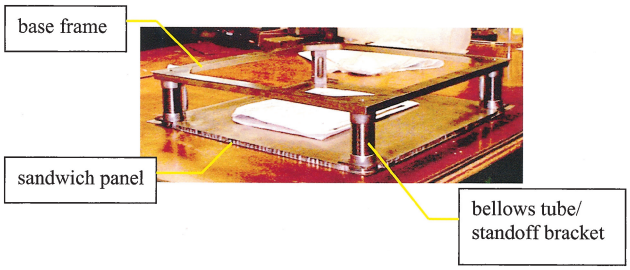

Fig. 25 TPS panel assembly without insulation and edge and bottom closeouts. (Panel is oriented upside down.)

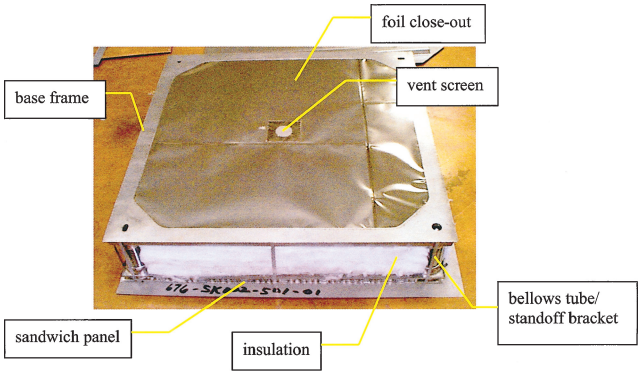

Fig. 26 TPS panel assembly with insulation and bottom CP Ti foil closeout installed (bottom view).

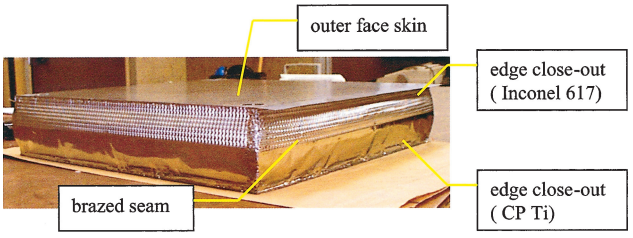

Fig. 27 Completed TPS panel with edge closeouts (side view).

reduced-pressure environments. Figure 26 shows the bottom view of the panel after the insulation was installed and the bottom was closed out. To complete the closeout of the top surface, removable Inconel 625 plugs and rings were machined and installed into the access holes in the honeycomb core sandwich panel.

The completed TPS panel is shown in Fig. 27. The panel edges were closed out with 0.002-in.-thick Inconel 600 foil and 0.002-in.-thick CP Ti foil. One end of the Inconel 600 foil was brazed to the underside of the outer face skin of the honeycomb core sandwich panel, and one end of the CP Ti foil was brazed to the base frame. The free ends of the Inconel 600 foil and the CP Ti foil were intercoiled together with braze foil along the midthickness and folded together at the corners of the TPS panel and brazed to form an airtight seam.

Coatings

An oxidation protection coating was applied to the external face skin of the TPS panels. The selected coating consisted of an alumina base layer and a two-phase glass (TPG) outer layer with a total thickness of approximately 200 μin. The alumina layer prevents interaction between the Inconel 617 face skin and the silica-based TPG coating layer. The alumina and TPG precursors were produced using sol-gel techniques and sprayed onto the panel face skin. The coating layers were cured individually in air at approximately 1100°F for 5 min using a radiant heat lamp array. Details of the development and oxidation protection behavior of the coating system are discussed in Refs. 17–19.

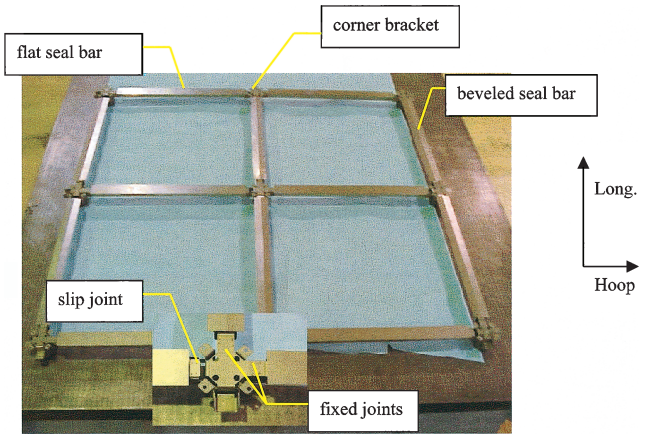

Fig. 28 Ti-6Al-4V interface hardware.

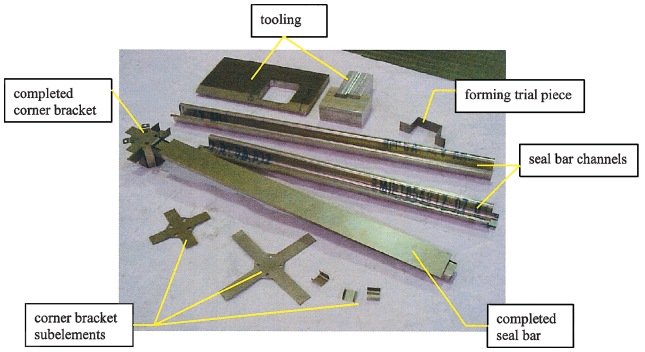

Fig. 29 Tooling, subelements, and channels used to fabricate Ti-6Al-4V corner brackets and seal bars for interface hardware.

TPS Support System

A picture of the TPSS hardware assembly is shown in Fig. 28. This hardware allows the attachment of a 2 × 2 array of flat TPS panels to a curved externally stiffened cryogenic tank panel. The bottom of the corner brackets are designed to be bolted to the caps of the tank panel T-stiffeners. The TPS panels rest on the seal bars and are bolted to the top of the corner brackets. A thin-gauge (0.012- and 0.016-in.) Ti-6Al-4V sheet was used to minimize the weight of the interface hardware components. The components were fabricated using conventional sheet metal forming and spot-welding techniques. Each component of the interface hardware consisted of multiple subelements that were cut to size, formed to the appropriate configurations, and spot welded together in order to provide the various flanges, slip joints, attachment points, and sealing surfaces.

Figure 29 shows some of the tooling, sheet metal subelements, and formed channels used to fabricate the seal bars and corner brackets. One completed corner bracket/seal bar assembly is also shown.

Summary

A new adaptable, robust, metallic, operable, reusable (ARMOR) thermal-protection-system (TPS) concept has been designed, analyzed, and fabricated. In addition to the inherent, tailorable robustness of metallic TPS, the ARMOR TPS offers improved features based on lessons learned from previous metallic TPS development efforts. ARMOR TPS panels can be attached directly to a smooth substructure or supported on TPS support structure above an externally stiffened or uneven substructure. Bulged, compliant sides minimize or eliminate radiation heat shorts in the panel-to-panel gaps. Innovative, internal support brackets provide a structural load path between the hot outer surface and cooler interior without causing unacceptable heat shorts, yet allow free thermal expansion of the outer surface. Cool, subsurface mechanical fasteners provide reliable, reusable attachments. The outer Inconel honeycomb sandwich facesheets can be readily thickened to achieve required levels of robustness.

A specific location on a single-stage-to-orbit reusable launch vehicle was selected to develop loads and requirements needed to design prototype ARMOR TPS panels. The design loads include ascent and entry heating rate histories, pressures, acoustic loads, and accelerations. Critical thermal/structural design loads were identified at eight points during the ascent and entry. Additional TPS design issues were identified and discussed.

An iterative sizing procedure was used to size the ARMOR TPS panels for thermal and structural loads as part of an integrated TPS/cryogenic tank structural wall. The TPS panels were sized to maintain acceptable temperatures on the underlying structure and to withstand the design structural loading. Detailed creep analyses were also performed on critical components of the ARMOR TPS panels. A TPS support system for connecting the ARMOR TPS panels to the externally stiffened cryogenic tank structure was also designed.

Four 18-in.-square ARMOR TPS panels and associated TPS support system hardware were fabricated. Materials, dimensions, and fabrication processes are described. Test plans for the fabricated hardware are presented.

Although much work remains to mature the ARMOR TPS concept, the initial efforts of the current study are encouraging. A plausible concept that addresses many of the anticipated TPS requirements and design goals has been designed, analyzed, and fabricated.

Acknowledgment

The authors gratefully acknowledge Richard Thompson of the Aerothermodynamics Branch at NASA Langley Research Center for providing the radiation equilibrium temperature distribution shown in Fig. 4.

References

[1]Cook, S. A., "The X-33 Advanced Technology Demonstrator," AIAA Paper 96-1195, April 1996.

[2]Blosser, M. L., "Advanced Metallic Thermal Protection Systems for Reusable Launch Vehicles," Ph.D. Dissertation, Dept. of Mechanical and Aerospace Engineering, Univ. of Virginia, Charlottesville, VA, May 2000.

[3]Dorsey, J. T., Poteet, C. C., Wurster, K. E., and Chen, R. R., "Metallic Thermal Protection System Requirements, Environments, and Integrated Concepts," *Journal of Spacecraft and Rockets*, Vol. 41, No. 2, 2004, pp. 162–172; also AIAA Paper 2002-0502, Jan. 2002.

[4]Bouslog, S. A., Moore, B., Lawson, I., and Sawyer, J. W., "X-33 Metallic TPS Tests in NASA-LaRC High Temperature Tunnel," AIAA Paper 99-1045, Jan. 1999.

[5]Blosser, M. L., Martin, C. J., Daryabeigi, K., and Poteet, C. C., "Reusable Metallic Thermal Protection Systems Development," *Proceedings of the 3rd European Workshop on Thermal Protection Systems*, ESTEC, Noordwijk, The Netherlands, 1998, pp. 165–176.

[6]Dorsey, John T., Myers, David E., and Martin, Carl J., "Reusable Launch Vehicle Tank/Intertank Sizing Trade Study," AIAA Paper 2000-1043, Jan. 2000.

[7]Poteet, C. C., Abu-Khajeel, H., and Hsu, S.-Y., "Preliminary Thermal–Mechanical Sizing of a Metallic Thermal Protection System," *Journal of Spacecraft and Rockets*, Vol. 41, No. 2, 2004, pp. 173–182; also AIAA Paper 2002-0505, Jan. 2002.

[8]Hender, D. R., "A Minature Version of the JA-70 Aerodynamic Heating Computer Program, H800 (MINIVER)," McDonnell Douglas Astronautics Co., MDC Rept. G0462, Huntington Beach, CA, June 1970 (revised Jan. 1972).

[9]Blosser, M. L., "Fundamental Modeling and Thermal Performance Issues for Metallic Thermal Protection System Concept," *Journal of Spacecraft and Rockets*, Vol. 41, No. 2, 2004, pp. 195–206; also AIAA Paper 2002-0503, 2002.

[10]Weiser, E. S., Johnson, T. F., St. Clair, T. L., Echigo, Y., Kaneshiro, H., and Grimsley, B. W., "Polyimide Foams for Aerospace Vehicles," *High Performance Polymers*, Vol. 12, No. 1, 2000, pp. 1–12.

[11]Chen, R. R., and Blosser, M. L., "Metallic Thermal-Protection-System Panel Flutter Study," *Journal of Spacecraft and Rockets*, Vol. 41, No. 2, 2004, pp. 207–212; also AIAA Paper 2002-0501, 2002.

[12]"MSC.Patran 2001 r2," MSC.Software Corp., Santa Ana, CA, 2001.

[13]"MSC/NASTRAN Quick Reference Guide Version 70.5," MacNeal-Schwendler Corp., Los Angeles, 1998.

[14]Brown, W., Jr., Mindlin, H., and Ho, C. (eds.), *Aerospace Structural Metals Handbook*, CINDAS/USAF CRDA Handbook Operation, Purdue Univ., West Lafayette, IN, 1994.

[15]Taminger, Karen M. B., "Analysis of Creep Behavior and Parametric Models for 2124 Al and 2124 Al + SiCw Composite," M.S. Thesis, Dept. of Materials Science and Engineering, Virginia Polytechnic Inst. and State Univ., Blacksburg, VA, Feb. 1999.

[16]"MSC.Marc 2001," MSC.Software Corp., Santa Ana, CA, 2001.

[17]Bird, R. K., Wallace, T. A., and Sankaran, S. N., "Effect of Oxidation on Properties and Microstructure of Candidate Alloys for Reusable Launch Vehicle Thermal Protection Systems," *Proceedings of the 25th Annual Conference on Composites, Materials, and Structures*, ZAI, Arlington, VA, 2001.

[18]Sankaran, S. N., Wiedemann, K. E., Bird, R. K., and Wallace, T. A., "Development of Protective Coatings for Thermal Protection Systems for Reusable Launch Vehicle Applications," *Proceedings of the 25th Annual Conference on Composites, Materials, and Structures*, ZAI, Arlington, VA, 2001.

[19]Bird, R. K., Wallace, T. A., and Sankaran, S. N., "Development of Protective Coatings for High-Temperature Metallic Materials," *Journal of Spacecraft and Rockets*, Vol. 41, No. 2, 2004, pp. 213–220.

S. A. Bouslog
Associate Editor

Color reproductions courtesy of NASA.